Journal of Molecular Structure 1184 (2019) 583–592

Contents lists available at ScienceDirect

Journal of Molecular Structure

journal homepage: http://www.elsevier.com/locate/molstruc

Efficient green synthesis of antioxidant azacoumarin dye bearing spiro-pyrrolidine for enhancing electro-optical properties of perovskite solar cells

S.K. Attia [c], A.T. Elgendy [b], S.A. Rizk [a, *]

[a] Chemistry Department, Faculty of Science, Ain Shams University, Cairo, Egypt
[b] Physics Department, Faculty of Science, Ain Shams University, Cairo, Egypt
[c] Egyptian Petroleum Research Institute, Evaluation and Analysis Department, Cairo, Egypt

ARTICLE INFO

Article history:
Received 22 November 2018
Received in revised form
10 February 2019
Accepted 11 February 2019
Available online 14 February 2019

Keywords:
Green synthesis
Spiro-heterocyclic
Azacoumarin
Perovskite solar cell

ABSTRACT

The challenge of increasing solar cell production in our life face with respect to the quality, efficiency, and environmental (eco-friendly) demand continuous improvement in solar cell study. Solar cells have emerged as powerful techniques for satisfying the increasing energy demand. One of the successful attitudes adopted in this field is using perovskite materials, which provide a cheap approach to be widely used in fabricating solar cells. For this reason, we focus in our work on enhancing the quality of perovskite materials in order to increase its efficiency towards light absorption and increase its photovoltaic behavior. Herein, different azacoumarin additives were prepared using a series of Spiro-indolone moieties and their structures were confirmed using Fourier transform infrared (FT-IR) spectroscopy and proton nuclear magnetic resonance (^{1}H-NMR). The prepared compounds have been subjected to quantum chemical calculations to investigate the molecular orbital parameters and to study their quantitative structure–activity and structure–property relationships. The obtained results have indicated that these compounds are promising in the field of dye-sensitized solar cells. More interestingly, these compounds have proven to be effective as antioxidants for lubricating oils. All these claims have been confirmed by experimental evidences.

1. Introduction

The development of lubricants has become a fundamental part of the development of machinery and its corresponding technologies. It is irrevocable and interdisciplinary linked to numerous fields of expertise and without this interdisciplinary aspect, lubricant improvements and applications would fail to achieve success [1]. Additives are synthetic chemicals used to improve different lubricant parameters, they can boost existing properties, reduce adverse characteristics, or introduce new properties in the base oil They can be added to base oils at percentage levels up to 5–30% of total weight [2]. The lubricating oils consist of hydrocarbons with (C20–C70) carbon atoms. At higher temperature, these hydrocarbons are oxidized to form alcohols, acids, aldehydes, esters, ketones and peroxides. All these compounds form the solid asphaltic materials. For this reason, the addition of antioxidants is necessary to all base stock oils to minimize the formation of such compounds [3]. Most of heterocyclic compounds containing active elements such as S, P, O and N which has compact structure possess antioxidant, anticorrosion and anti-wear properties [4] Strong interaction between additive molecules and metal surfaces is an essential requirement for excellent tribological performance [5]. Organic molecules usually promote the formation of a chelate compound on the metal surface by donating electrons to the latter. In this regard, the metal acts as an electrophile and the heteroatoms of the organic additives, rich in lone pairs of electrons, act as nucleophiles and thus coordinate covalent bonds are formed [6].

Bulk Heterojunction (BHJ) organic solar cell using solution-processed small molecules as donors have contained within the relatively simple synthesis and purification, well-defined structures, non-toxins, high charge carrier mobility and less batch-to batch variation [7,8]. The power conversion efficiencies (PCEs) of solar cells using small molecules as donors have exceeded 20% as ideal candidates for solution-processed organic solar cells [9].

* Corresponding author.
E-mail address: samehrizk@sci.asu.edu.eg (S.A. Rizk).

https://doi.org/10.1016/j.molstruc.2019.02.042
0022-2860/

Solution-processed organic solar cells have been broadly investigated due to their unique features, such as light weight, mechanical elasticity, large area handling and engineering low-cost. A significant increase in expedient performance has attained via use of solid-state hole transport materials, for example, 2,2,7,7-tetra-kis-(N, N-di-4-methoxyphenylamino)-9,9-spirobifuorene more commonly referred to in the literature as Spiro-OMe-TAD [10,11]. The PCE solid state has flown from 9.7% in 2012 to 22.1% in 2017 [12]. Despite the simplicity of the original Perovskite crystal structures, this family of compounds shows an enormous variety of structural modifications and variants of magnetic and electric properties due to it contain magnetic properties "colossal magnetoresistance" which means their electrical resistance can be changed in the presence of the magnetic field, some perovskite structures can be used as the superconductors, where a material can conduct electricity with no resistance, such as $LaGaO_3$, $PrGaO_3$ and $NdGaO_3$ [12,13]. Finally, ionic conductors, which mean atoms inside the structure, can move around without the whole thing falling apart. This is particularly useful for fabrications energy, materials such as solar cells and batteries.

DFT method is among the best commonly used computational methodologies for predicting the chemical reactivity of molecules and solids. It is an efficient approach that can be effective to provide insights into the chemical reactivity of organic compounds [14]. DFT uses a quantum methodology with a relatively small machine time and good accuracy, and this is because instead of using the whole system' s electrons, it uses only the electron density of the molecule [15].

In the present work, different Azacoumarin additives were prepared and it was allowed to react with a series of Spiro-indolone moieties afforded the grades of dye. The efficiency of the prepared compounds as antioxidants additive for lubricating oil was investigated. Moreover, enhance the quality of perovskite materials in order to increase its efficiency of absorption of wavelength and increase its photovoltaic behavior.

2. Material and methods

2.1. Synthetic procedures

All melting points are corrected and determined on a Stuart electric melting point apparatus (Microanalytical center, Ain shams university, Cairo, Egypt). Elemental analyses were carried out by Elementary Viro El-Microanalysis at the Micro-Analytical Center, National Research Center, Egypt. IR spectra (KBr) were recorded on infrared spectrometer FT-IR 400D (New York, NY, USA) using OMNIC program and are reported wave number of absorptions in terms of cm^{-1} and ^{1}H-NMR spectra recorded on a Bruker spectrophotometer (Rheinstetten, Germany) at 400 MHz using TMS as internal standard and with residual signals of the deuterated solvent δ 2.51 ppm for DMSO-d_6. Homogeneity of all synthesized compounds was checked by TLC.

3,4-Dichlorophenyl-4′-phenyl-1′-methyl-spiro[indoline-3,2′-pyrrolidin]-3′yl) methanone (1a). Recrystallized from toluene, colorless solid, 65% (r.t.), m.p. 202–204 °C; IR (KBr), υ, cm^{-1}: 3370, 3323(NH), 3052 (CH_{Ar}), 1692, 1670 (C=O) cm^{-1}; ^{1}H NMR (400 MHz, DMSO-d_6), δ, ppm, (J, Hz): 2.18 (3H, s, NCH_3), 2.84–2.93 (2H, m, CH_2), 3.7 (1H, q, $J = 8.4$ Hz, CHPh), 4.23 (1H, d, $J = 8.4$ Hz, CHCOAr), 7.36 (3H, dd, $J = 8.4$ Hz, 3,4,5-CH(Ph)), 7.40 (2H, s, 1,4-CH (indol)), 7.41 (2H, d, 2,3-CHindol), 7.43 (2H, dd, $J = 8.4$ Hz, 2,6-CH (Ph)), 7.52–7.50 (1H, dd, $J = 8.4$ Hz, 5-CH(Cl_2ph)), 7.72–7.69 (1H, dd, $J = 9.2$ Hz, 6-CH(Cl_2ph)), 7.84–7.92 (1H, d, $J = 9.2$ Hz, 2-CH(Cl_2ph)), 10.45 (1H, s, 1-NH); found, %: C 66.54, H 4.45, Cl 15.70, N 6.20 for $C_{25}H_{20}Cl_2N_2O_2$ (450). Calculated,%: C 66.53, H 4.47, Cl 15.71, N 6.21.

4-Bromophenyl-4'-(4-chlorophenyl)-1′-methyl-spiro[indoline-3,2′-pyrrolidin]-3′yl-methanone (1b). Recrystallized from toluene, colorless solid, 72% (r.t.), m.p.206–208 °C; IR (KBr), υ, cm^{-1}: 3354, 3270(NH), 3052 (CH_{Ar}), 1692, 1669 (C=O) cm^{-1}; ^{1}H NMR (400 MHz, DMSO-d_6), δ, ppm, (J, Hz): 2.18 (3H, s, NCH_3), 2.94–2.98 (2H, m, CH_2), 3.37 (1H, q, $J = 8.4$ Hz, CH(ClPh)), 4.23 (1H, d, $J = 8.4$ Hz, CHCO(BrPh)), 7.21 (2H, dd, $J = 8.1$ Hz, 5-2,6-CH(ClPh)), 7.36 (2H, d, $J = 8.4$ Hz, 3,5-CH(ClPh)), 7.40 (2H, s, 1,4-CH (indol)), 7.41 (2H, d, 2,3-CHindol), 7.52–7.50 (2H, dd, $J = 9.2$ Hz, 2,6-CH(Brph)), 7.72–7.69 (2H, dd, $J = 9.2$ Hz, 3,5-CH(Brph)), 10.45 (1H, s, 1-NH); found, %: C 60.55, H 4.05, Br 16.10, Cl 7.14, N 5.63 for $C_{25}H_{20}BrClN_2O_2$ (494). Calculated, %: C 60.56, H 4.07, Br 16.12, Cl 7.15, N 5.65.

(4'-(4-Chlorophenyl)-1′-methyl-spiro[indoline-3,2′-pyrrolidin]-3′yl) (3,4-dimethyl phenyl) methanone (1c). Recrystallized from toluene, colorless solid, 57% (r.t.), m.p.194–196 °C; IR (KBr), υ, cm^{-1}: 3322, 3198(NH), 3052 (CH_{Ar}), 1690, 1667 (C=O) cm^{-1}; ^{1}H NMR (400 MHz, DMSO-d_6), δ, ppm, (J, Hz): 2.02 (6H, s, $2CH_3$(Ph)), 2.18 (3H, s, NCH_3), 2.84–2.93 (2H, m, CH_2), 2.97 (1H, q, $J = 8.4$ Hz, CH(ClPh)), 4.13 (1H, d, $J = 8.4$ Hz, CHCOAr), 6.91 (1H, d, $J = 8.1$ Hz, 5-CH(Ar)), 7.36 (1H, s, 2-CH(Ar)), 7.40 (2H, s, 1,4-CH (indol)), 7.41 (2H, d, 2,3-CHindol), 7.43 (1H, s, 6-CH(Ar)), 7.52–7.50 (2H, dd, $J = 8.4$ Hz, 2,6-CH(Clph)), 7.72–7.69 (2H, dd, $J = 9.2$ Hz, 3,5-CH(Clph)), 10.45 (1H, s, 1-NH); found, %: C 72.86, H 5.64, Cl 7.94, N 6.27 for $C_{27}H_{25}ClN_2O_2$ (444). Calculated, %: C 72.88, H 5.66, Cl 7.97, N 6.30.

N-(4-(4'-(4-Chlorophenyl-1′-methyl-spiro[indoline-3,2′-pyrrolidin]-3′-carbonyl) phenyl) acetamide (1d) Recrystallized from toluene, colorless solid, 40% (r.t.), m.p.210–212 °C; IR (KBr), υ, cm^{-1}: 3348, 3280(NH), 3050 (CH_{Ar}), 1691, 1669 (C=O) cm^{-1}; ^{1}H NMR (400 MHz, DMSO-d_6), δ, ppm, (J, Hz): 2.18 (3H, s, NCH_3), 2.33(3H, s, CH_3CO), 2.84–2.95 (2H, m, CH_2N), 2.99–3.02 (1H, q, $J = 8.4$ Hz, CH(ClPh)), 3.92–4.02 (1H, d, $J = 8.4$ Hz, CHCOAr), 6.91–6.97 (2H, d, $J = 8.1$ Hz, 2,6-CH(Ar)), 7.16 (2H, dd, $J = 8.4$ Hz, 3,5-CH(Ar)), 7.40 (2H, s, 1,4-CH (indol)), 7.41 (2H, d, 2,3-CHindol), 7.43 (2H, dd, $J = 8.4$ Hz, 3,5-CH(ClPh)), 7.72–7.69 (2H, dd, $J = 9.2$ Hz, 2,6-CH(Clph)), 10.45 (1H, s, 1-NH), 10.72(1H, s, NHacet); found,%: C 68.43, H 5.09, Cl 7.50, N 8.85 for $C_{27}H_{24}ClN_3O_3$ (473). Calculated, %: C 68.42, H 5.10, Cl 7.48, N 8.87.

N-(4-(1′-Methyl-4'-(4-nitrophenyl-spiro[indoline-3,2′-pyrrolidin]-3′-carbonyl) phenyl) acetamide (1e). Recrystallized from toluene, off white solid, 64% (r.t.), m.p. 236–238 °C; IR (KBr), υ, cm^{-1}: 3349, 3317(NH), 3052 (CH_{Ar}), 1695, 1671 (C=O) cm^{-1}; ^{1}H NMR (400 MHz, DMSO-d_6), δ, ppm, (J, Hz): 2.18 (3H, s, NCH_3), 2.31(3H, s, CH_3CO), 2.78–2.83 (2H, m, CH_2N), 4.01 (1H, q, $J = 8.4$ Hz, CH($PhNO_2$), 4.13 (1H, d, $J = 8.4$ Hz, CHCOAr), 6.96 (1H, d, $J = 8.1$ Hz, 2,6-CHAr), 7.16 (2H, d, $J = 8.4$ Hz, 3,5-CHAr), 7.40 (2H, s, 1,4-CH (indol)), 7.41 (2H, d, 2,3-CHindol), 7.43 (2H, dd, $J = 8.4$ Hz, 3,5-CH (NO_2Ph)), 7.72–7.69 (2H, dd, $J = 9.2$ Hz, 2,6-(CHPh)), 10.45 (1H, s, 1-NH), 10.74(1H, s, NH which exchange in D_2O); found, %: C 66.90, H 4.98, N 11.55 for $C_{27}H_{24}N_4O_5$ (484). Calculated, %: C 66.93, H 4.99, N 11.56.

7-(3′-Benzoyl-4'-(3,4-dichlorophenyl)-1′-methylspiro [indole-3,2′-pyrrolidin]-2-yl) oxy)-4-phenyl-2H-chromen-2-one (2). Recrystallized from toluene, colorless solid, 65% (r.t.), m.p. 202–204 °C; IR (KBr), υ, cm^{-1}: 3370, 3323(NH), 3052 (CH_{Ar}), 1692, 1670 (C=O) cm^{-1}; ^{1}H NMR (400 MHz, DMSO-d_6), δ, ppm, (J, Hz): 2.18 (3H, s, NCH_3), 2.84–2.93 (2H, m, CH_2), 3.7 (1H, q, $J = 8.4$ Hz, CHPh), 4.23 (1H, d, $J = 8.4$ Hz, CHCOAr), 7.36 (3H, dd, $J = 8.4$ Hz, 3,4,5-CH(Ph)), 7.40 (2H, s, 1,4-CH (indol)), 7.41 (2H, d, 2,3-CHindol), 7.43 (2H, dd, $J = 8.4$ Hz, 2,6-CH (Ph)), 7.52–7.50 (1H, dd, $J = 8.4$ Hz, 5-CH(Cl_2ph)), 7.72–7.69 (1H, dd, $J = 9.2$ Hz, 6-CH(Cl_2ph)), 7.84–7.92 (1H, d, $J = 9.2$ Hz, 2-CH(Cl_2ph)), 10.45 (1H, s, 1-NH); found, %: C 66.54, H 4.45, Cl 15.70, N 6.20 for $C_{25}H_{20}Cl_2N_2O_2$ (450). Calculated,%: C 66.53, H 4.47, Cl 15.71, N 6.21.

7-(4'-(4-Bromophenyl)-3'-(4-chlorobenzoyl)-1′-methylspiro

[indole-3,2′-pyrrolidin] -2-yl) oxy)-4-phenyl-2H-chromen-2-one (3). Recrystallized from toluene, colorless solid, 72% (r.t.), m.p.206–208 °C; IR (KBr), υ, cm^{-1}: 3354, 3270(NH), 3052 (CH_{Ar}), 1692, 1669 (C=O) cm^{-1}; ^1H NMR (400 MHz, DMSO-d_6), δ, ppm, (J, Hz): 2.18 (3H, s, NCH_3), 2.94–2.98 (2H, m, CH_2), 3.37 (1H, q, $J = 8.4$ Hz, CH(ClPh)), 4.23 (1H, d, $J = 8.4$ Hz, CHCO(BrPh)), 7.21 (2H, dd, $J = 8.1$ Hz, 5-2,6-CH(ClPh)), 7.36 (2H, d, $J = 8.4$ Hz, 3,5-CH(ClPh)), 7.40 (2H, s, 1,4-CH (indol)), 7.41 (2H, d, 2,3-CHindol), 7.52–7.50 (2H, dd, $J = 9.2$ Hz, 2,6-CH(Brph)), 7.72–7.69 (2H, dd, $J = 9.2$ Hz, 3,5-CH(Brph)), 10.45 (1H, s, 1-NH); found, %: C 60.55, H 4.05, Br 16.10, Cl 7.14, N 5.63 for $C_{25}H_{20}BrClN_2O_2$ (494). Calculated, %: C 60.56, H 4.07, Br 16.12, Cl 7.15, N 5.65.

7-(3'-(4-chlorobenzoyl)-4'-(3,4-dimethylphenyl)-1′-methylspiro[indole-3,2′-pyrrolidin]-2-yl) oxy)-4-phenyl-2H-chromen-2-one (4). Recrystallized from toluene, colorless solid, 57% (r.t.), m.p.194–196 °C; IR (KBr), υ, cm^{-1}: 3322, 3198(NH), 3052 (CH_{Ar}), 1690, 1667 (C=O) cm^{-1}; ^1H NMR (400 MHz, DMSO-d_6), δ, ppm, (J, Hz): 2.02 (6H, s, $2CH_3$(Ph)), 2.18 (3H, s, NCH_3), 2.84–2.93 (2H, m, CH_2), 2.97 (1H, q, $J = 8.4$ Hz, CH(ClPh)), 4.13 (1H, d, $J = 8.4$ Hz, CHCOAr), 6.91 (1H, d, $J = 8.1$ Hz, 5-CH(Ar)), 7.36 (1H, s, 2-CH(Ar)), 7.40 (2H, s, 1,4-CH (indol)), 7.41 (2H, d, 2,3-CHindol), 7.43 (1H, s, 6-CH(Ar)), 7.52–7.50 (2H, dd, $J = 8.4$ Hz, 2,6-CH(Clph)), 7.72–7.69 (2H, dd, $J = 9.2$ Hz, 3,5-CH(Clph)), 10.45 (1H, s, 1-NH); found, %: C 72.86, H 5.64, Cl 7.94, N 6.27 for $C_{27}H_{25}ClN_2O_2$ (444). Calculated, %: C 72.88, H 5.66, Cl 7.97, N 6.30.

7-(4'-(4-Acetylaminophenyl)-3'-(4-chlorobenzoyl)- 1′-methylspiro[indole-3,2′-pyrrolidin]-2-yl)oxy)-4-phenyl-2H-chromen-2-one (5) Recrystallized from toluene, colorless solid, 40% (r.t.), m.p.210–212 °C; IR (KBr), υ, cm^{-1}: 3348, 3280(NH), 3050 (CH_{Ar}), 1691, 1669 (C=O) cm^{-1}; ^1H NMR (400 MHz, DMSO-d_6), δ, ppm, (J, Hz): 2.18 (3H, s, NCH_3), 2.33(3H, s, CH_3CO), 2.84–2.95 (2H, m, CH_2N), 2.99–3.02 (1H, q, $J = 8.4$ Hz, CH(ClPh)), 3.92–4.02 (1H, d, $J = 8.4$ Hz, CHCOAr), 6.91–6.97 (2H, d, $J = 8.1$ Hz, 2,6-CH(Ar)), 7.16 (2H, dd, $J = 8.4$ Hz, 3,5-CH(Ar)), 7.40 (2H, s, 1,4-CH (indol)), 7.41 (2H, d, 2,3-CHindol), 7.43 (2H, dd, $J = 8.4$ Hz, 3,5-CH(ClPh)), 7.72–7.69 (2H, dd, $J = 9.2$ Hz, 2,6-CH(Clph)), 10.45 (1H, s, 1-NH), 10.72(1H, s, NHacet); found,%: C 68.43, H 5.09, Cl 7.50, N 8.85 for $C_{27}H_{24}ClN_3O_3$ (473). Calculated, %: C 68.42, H 5.10, Cl 7.48, N 8.87.

7-(4'-(4-Acetylaminophenyl)-3'-(4-nitrobenzoyl)-1′-methylspiro[indole-3,2′-pyrrolidin]-2-yl) oxy)-4-phenyl-2H-chromen-2-one (6). Recrystallized from toluene, off white solid, 64% (r.t.), m.p. 236–238 °C; IR (KBr), υ, cm^{-1}: 3349, 3317(NH), 3052 (CH_{Ar}), 1695, 1671 (C=O) cm^{-1}; ^1H NMR (400 MHz, DMSO-d_6), δ, ppm, (J, Hz): 2.18 (3H, s, NCH_3), 2.31(3H, s, CH_3CO), 2.78–2.83 (2H, m, CH_2N), 4.01 (1H, q, $J = 8.4$ Hz, CH($PhNO_2$), 4.13 (1H, d, $J = 8.4$ Hz, CHCOAr), 6.96 (1H, d, $J = 8.1$ Hz, 2,6-CHAr), 7.16 (2H, d, $J = 8.4$ Hz, 3,5-CHAr), 7.40 (2H, s, 1,4-CH (indol)), 7.41 (2H, d, 2,3-CHindol), 7.43 (2H, dd, $J = 8.4$ Hz, 3,5-CH (NO_2Ph)), 7.72–7.69 (2H, dd, $J = 9.2$ Hz, 2,6-(CHPh)), 10.45 (1H, s, 1-NH), 10.74(1H, s, NH which exchange in D_2O); found, %: C 66.90, H 4.98, N 11.55 for $C_{27}H_{24}N_4O_5$ (484). Calculated, %: C 66.93, H 4.99, N 11.56.

2.2. Oxidation stability study

The physicochemical properties of the delivered base stock oil were carried out according to ASTM standard test methods. The results were tabulated in Table 2. The oxidation test was carried out according to ASTMD-943 standard method. The oxidation cell in the static mode contained 200 ml base stock, and iron and copper wires as catalysts. The base stock sample was subjected to oxidation at 120 °C with pure oxygen (99.95%) at a flow rate of 0.1 L/hour for maximum 96 h. The characterized compounds were added with different concentrations (200, 400 and 500 ppm). The oil samples were examined (after 24, 48, 72 and 96 h, respectively) change in total acid number (TAN).

2.3. Molecular polarizability

The molecular polarizability α_p is obtained from the equation of Clausius and Mossotti resp. which take the form

$$\alpha_p = \left(\frac{n^2-1}{n^2+2}\right)\left(3\frac{\in 0M}{N_A\rho}\right) \quad (1)$$

The Lorentz-Lorenz formula describes the dependence of the refractive index n on the density ρ, the molar mass M and of the medium. N_A denotes Avogadro's number and ε_0 the vacuum permittivity.

2.4. Calculation details

DMol3 module in Materials Studio 6.0 (MS6.0) software from Accelrys, Inc., was employed to perform the DFT calculations using Pardew and Wang LDA exchange-correlation functional and DND basis set. The calculated parameters involved the Frontier molecular orbitals, dipole moment, Fukui indices and Mullikan atomic charges. Frontier molecular orbitals for each molecule include the highest occupied molecular orbital (HOMO) and the lowest unoccupied molecular orbital (LUMO). Molecular dynamics (MD) simulation was carried out to illustrate the adsorption of the studied molecules on the surface of Pb (110) at the molecular level using for citing Module and Compass forcefield in MS6.0 software. The crystals of perovskite adsorbent were constrained to avoid the disturbance of its atoms throughout the simulation process. Temperature was fixed at 298 K, with NVE (microcanonical) ensemble, with a time step of 1 fs and a simulation time of 5 ps. The calculated binding energy (E bind), expressing the interaction between each molecule and Pb surface, was calculated using the following equation:

$$\text{E binding} = \text{E tot} - (\text{E sorbent} + \text{E sorbate}) \quad (1a)$$

where E tot represents the total energy of the most stable configuration of each molecule of dye over perovskite. E sorbent and E sorbate represent the energies of individual perovskite surface and unbound molecules, respectively.

3. Results and discussion

3.1. Chemistry

High performance perovskite solar cells (PVSCs) have described with both meso-porous structures and planar heterojunction buildings with power conversion efficiency (PCE) over 15% [16–20]. Mesoporous structure devices usually require high temperature (over 450 °C) processing, which hinders their applications on typical glass or polymer substrates [21]. While the planar structure devices, which employ organic semiconductors as hole and electron transporting layer, can be fabricated at low temperature, offering a wide choice of substrates, electrodes and interfacial materials [22]. One-step spin-coating, two-step sequential deposition [23] and vapor-assisted solution process [24], have been developed for preparing perovskite films. Both one-step, spin-coating and two-step sequential deposition are all-solution-processes, which are compatible for large scale, cost-effective manufacturing. In the simple one-step, spin-coating method, a metal halide (lead iodide (PbI_2) or lead chloride ($PbCl_2$)) is dissolved with methylammonium iodide (MAI) in a polar solvent (such as dimethylformamide (DMF)) as the precursor solution. This solution is then spin-casted onto the substrate, followed by thermal annealing to form the perovskite layer. Nevertheless, discontinuous

perovskite films with pinholes are usually obtained, leading to current leakage and limiting the device performance [25]. Besides, relatively long annealing time (typically 1–2 h) is required for the formation of perovskite [26]. In the two-step sequential method, PbI_2 solution is first spin-casted onto the substrate, followed by dipping into or spin-coating MAI solution to produce the perovskite layer. Although this two-step method provides better control over the film morphology, a porous scaffold is needed for the complete transformation of PbI_2 into perovskite layer. Incomplete conversion of PbI_2 usually exists in planar structure, which causes problem in device reproducibility [27]. To achieve better performance, many different approaches have been developed to further improve the quality of the perovskite films, adding various additives [28]. The purpose of the present work is to investigate photovoltaic properties and microstructures of photovoltaic devices with perovskite-type $(CH_3NH_3Pb)_x$ (organic dye)$_{1-x}$ compounds, which were prepared by a simple spin-coating technique in air [29]. The multi-component 1,3-dipolar cycloaddition (MCDC) of azomethine ylides, generated in situ via decarboxylative condensation of isatin and α-amino acids with olefinic and acetylenic dipolarophiles, represents a key approach for the Regio specific construction of a variety of Spiro-oxindoles (Schemes 1 and 2). This route has become significant in combinatorial chemistry due to its process simplicity, mild conditions, atomic economy and the extension of the scope of substrates. The three-component condensation of equimolar amounts of isatin, sarcosine and chalcones in boiling aqueous methanol (1:3) afforded the Spiro oxindoles **1a-e** in moderate to excellent yields (Table 1). Spiro-oxindoles **1a-e** were exclusively formed and all newly cyclo-adducts were obtained by the above method were characterized by ^{1}H NMR and elemental analyses [28]. The regiochemical outcome of the cycloaddition was unambiguously confirmed by ^{1}H-NMR and ^{13}C-NMR [30]. Since the stereochemistry of the cycloadducts **1e** was clarified by a single-crystal X-ray analysis, and the mechanism of the azomethine ylide formation by a decarboxylative route has been repeatedly described [31–33] (Scheme 2). The Spiro-oxindole derivatives **1a-e**

Table 1
Three-component synthesis of spirooxindoles 1a-e.

Entry	Compounds	R_1	R_2	R_3	R_4	Reflux		Reaction in (r.t.)	
						time	yield%	time	Yield%
1	**1a**	H	Cl	Cl	H	1 h	37	11 h	65
2	**1b**	H	H	Br	Cl	1 h	50	8 h	72
3	**1c**	H	CH_3	CH_3	Cl	3 h	25	12 h	57
4	**1d**	NO_2	H	$NHCOCH_3$	Cl	1 h	34	5 h	40
5	**1e**	H	H	$NHCOCH_3$	NO_2	1 h	40	4 h	64

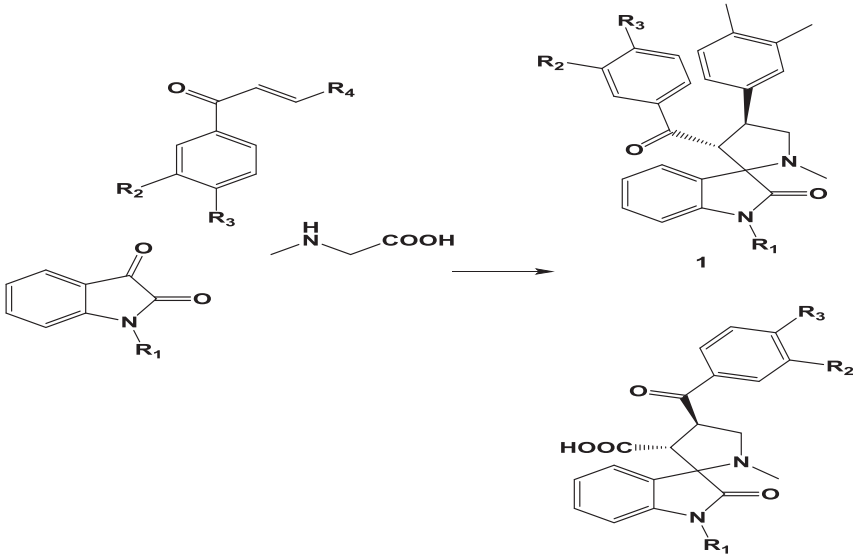

Scheme 1. Outline Regiospecific cycloaddition reaction of isatin, sacrosine, and aroylacrylic or chalcones via simple 1,3-dipolar.

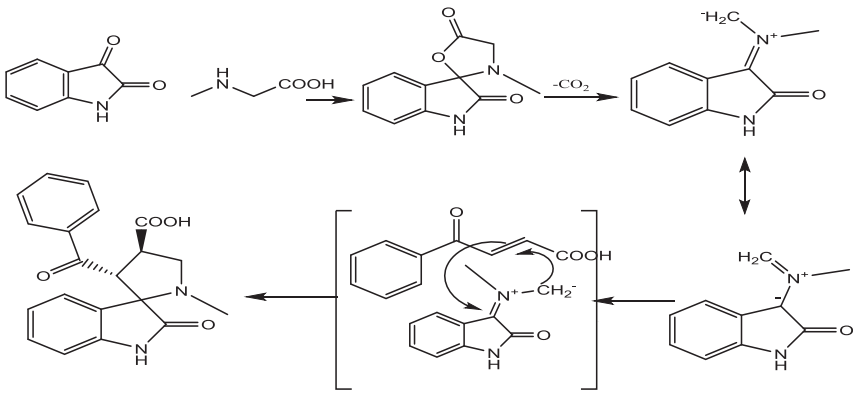

Scheme 2. Outline the mechanistic reaction of 1,3-dipolar and dipolarophile.

Table 2
Physicochemical characteristics of the base stock.

TEST		Test method	Result
Density At 15.5 °C, g/L		ASTM D – 4052	0.8916
Pour Point, ^{0}C		ASTM D - 97	−3
Viscosity	40 °C	ASTM D - 445	170.5
	100 °C	ASTM D - 445	15.03
Viscosity Index (VI)		ASTM D - 2270	86
Total Acid Number (TAN)		ASTM D - 664	0.028
Sulfur Content, wt %		ASTM D - 4294	0.59
Carbon Residue, wt %		ASTM D - 524	0.7
Ash Content, wt %		ASTM D - 482	0.004
Wax Content, wt %		UOP 46	0.87
Copper Corrosion		ASTM D-190	I a
Water Content, PPM		ASTM D-1744	50
Flash point, ^{0}C		ASTM D-9	244

were allowed to react with 7-hydroxy 4-phenyl-8-azacoumarin in the presence of phosphorous oxy chloride afforded the Spiro-Azacoumarin dye **2**–**6** (Schemes 3 and 4). Solution-processed organic solar cells (OSCs) have been broadly considered due to their unique features, such as light weight, mechanical flexibility, large area coverage and low-cost manufacturing [34–36]. The molecule exhibits good thermal stability and deep HOMO levels (Fig. 1). Small molecule donors include relatively simple synthesis and purification, well-defined structures, no end group contaminants, high charge Carrie mobility and less batch-to-batch variation [37–39]. This molecule exhibits good thermal stability with a decomposition temperature (5% weight loss) of 353 °C. The high thermal stability of the SPCD prevents the deformation of the molecule morphology and degradation of the active layer of small molecular solar cells. The dye exhibits better light-harvesting properties at wavelengths comparable to those of P3HT and an energy cascade that is compatible with P3HT and PCBM for both LUMO and HOMO energy levels. However, both the photocurrent and cell efficiency increase with increasing Coumarin dye.

3.2. Evaluation of the prepared compounds as antioxidants

Oxidation is the most predominant reaction of lubricant in service; it is responsible for several lubricant problems. These problems, including increase in total acid number, varnish, sludge and sediment formation, additive depletion. The data of the oxidation of base stock shown in the Table 3 showed that without adding additives, the total acid number increases from 0.028 mg KOH/g sample at room temperature to 0.94, 1.02, 1.20 and 2.02 mg KOH/g sample when thermally oxidized for 24, 48, 72 and 96 h respectively. The addition of additives showed a noticeable decrease in total acid numbers. The characterized compounds were added with different concentrations (200, 400 and 500 ppm). The data reveals that the most effective concentration in case of compounds (dyes 2–6) is 200 ppm. The order of increasing inhibition efficiency of Azacoumarin derivatives were ranked as follows: Dye**6** > Dye**5** >Dye **4** > Dye**3** > Dye**2** which were consistent with order of higher efficiency.

3.3. Electro-optical properties

Physical properties of our material isotropic optical materials such as cubic crystals and amorphous liquid or solids have only one refractive index because the atoms are arranged in three-dimensional symmetric way. In addition, the physical properties are the same in different direction. Where atoms in anisotropic materials are arranged in asymmetric way the physical property is different in different directions. In our study our liquid dyes of perovskite materials are isotropic material. The optical density (refractive index) of these transparent media is $n = \frac{c}{v} = \sqrt{\frac{\mu_0\ \varepsilon_0}{\mu\ \varepsilon}}$ where, $\mu_0\ \varepsilon_0$ are the vacuum permeability and permittivity and $\mu\ \varepsilon$ are the permeability and permittivity of the perovskite materials. The relationship between the refractive index n and wavelength of light λ for a particular transparent material are obtained from Cauchy's equation which take the form

$$n(\lambda) = a + \frac{b}{\lambda^2} \tag{2}$$

Where, Cauchy's equation is an empirical relationship between the refractive index n, wavelength of light λ for a particular transparent material and a,b are coefficient that can determined for material by fitting the equation to measured the refractive index at known wavelength (see Fig. 2). It is named for the mathematician

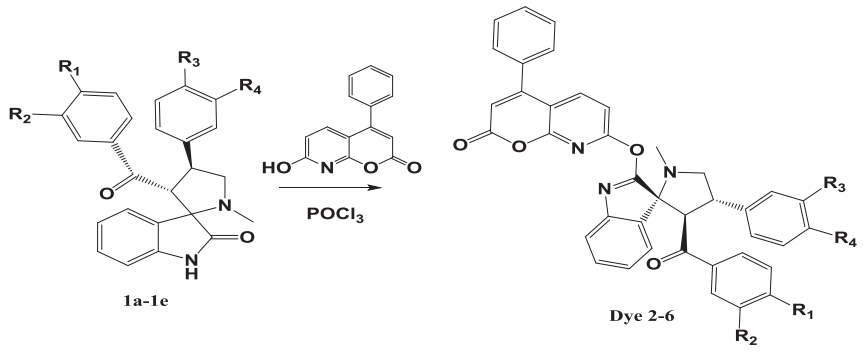

Scheme 3. Outline the chlorination reaction of spiroindoline followed by reaction with coumarin to form the dye 2-6.

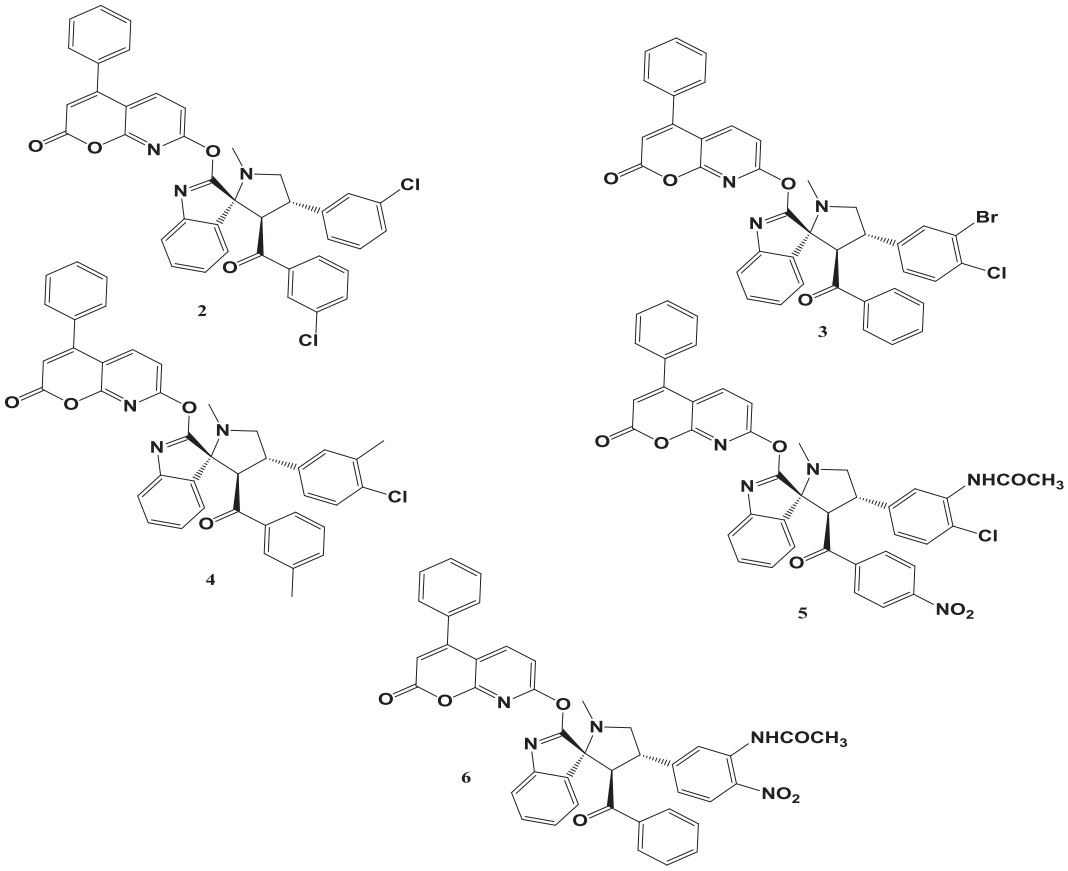

Scheme 4. Outline the chemical structure of Spiro-Azacoumarin dye (SACD).

Augustin Louis Cauchy. Comparison of all refractive index [40] (Tables 3 and 4; Figs. 3 and 4).

$$\alpha_p = \left(\frac{n^2-1}{n^2+2}\right)\left(3\frac{\varepsilon 0\, M}{N_A\, \rho}\right) \quad (3)$$

To describe the result of three relation of wavelength, absorption (Experimental results) and polarizability (theoretical by the value of Mossotti equation). The following equation outline the Best fitting is relates the Decca x of the power 10

$$De(x,y) = 15 - 2.7x + 1.9\times 10^{-7}x^{10} + 12.3y - 4xy + 0.00000125x^{9}y + 7y^{3} \quad (4)$$

Fitting curve is made by mathematical program and the results are given three dimensions of the two variable parameters (wavelength λ (x) and absorption α (y)). The best fitting of the following equation shows high non-linearity depending on wavelength and absorption (xy and x^5y) of the higher order of power five of the wavelength that means the polarizability is depending on the wavelength, absorption and multiple of absorption-wavelength.

The relation of wavelength, absorption and polarizability as outline in three-dimensional relation in Fig. 4. The numerical result gives a good approximation at x to the power 10 and non-linearity depending xy and x^5y. So, these parameters can be confirmed that the sensitized Dyes 4, 5 and 6 are characterized in range the visible light region and they are having good absorption and polarizability.

3.4. DFT-based characterization

Quantum chemistry methods and molecular modeling techniques enable the definition of a large number of molecular orbital (MO) descriptors characterizing, shape, the reactivity and binding properties of a complete molecule as well as of molecular fragments and substitutes [41]. Quantum chemical parameters calculations using density functional theory (DFT) method used for the calculations of the synthesized additive compounds the data show in Table 5. The high E_{HOMO} are likely to indicate a strong tendency of the molecule to donate electrons. Low absolute values of the energy band gap (ΔE) gives good inhibition efficiencies because the energy required to remove an electron from the last occupied orbital ($\Delta E = E_{LUMO} - E_{HOMO}$). The results obtained by Quantum chemical parameters calculations using density functional theory (DFT) method showed that, (**Dye 6**; ΔE = 0.26), (**Dye 5**; ΔE = 0.53), (**Dye 4**; ΔE = 2.5), (**Dye 3**; ΔE = 2.19), (**Dye 2**; ΔE = 2.35). According to these values, the efficiency order is as follows Dye**6** > Dye**5** >Dye **4** > Dye**3** > Dye**2** which shows good correlation with the prediction results obtained by quantum chemistry calculations and experimental.

DFT-based quantum calculations can give insights into the structural and electronic characteristics of organic molecules [42]. Herein, the parameters obtained from a DFT study performed for Spiro-Azacoumarin derivatives are the energies of Frontier molecular orbitals. HOMOs are the regions at which electrophilic attack occurs, whereas the LUMO represent the sites of nucleophilic attack [43]. The HOMO energy (E_{HOMO}) is a parameter of a direct relation to the ionization potential and its value expresses the susceptibility of organic molecule towards attacks by electrophiles. Unlikely, the

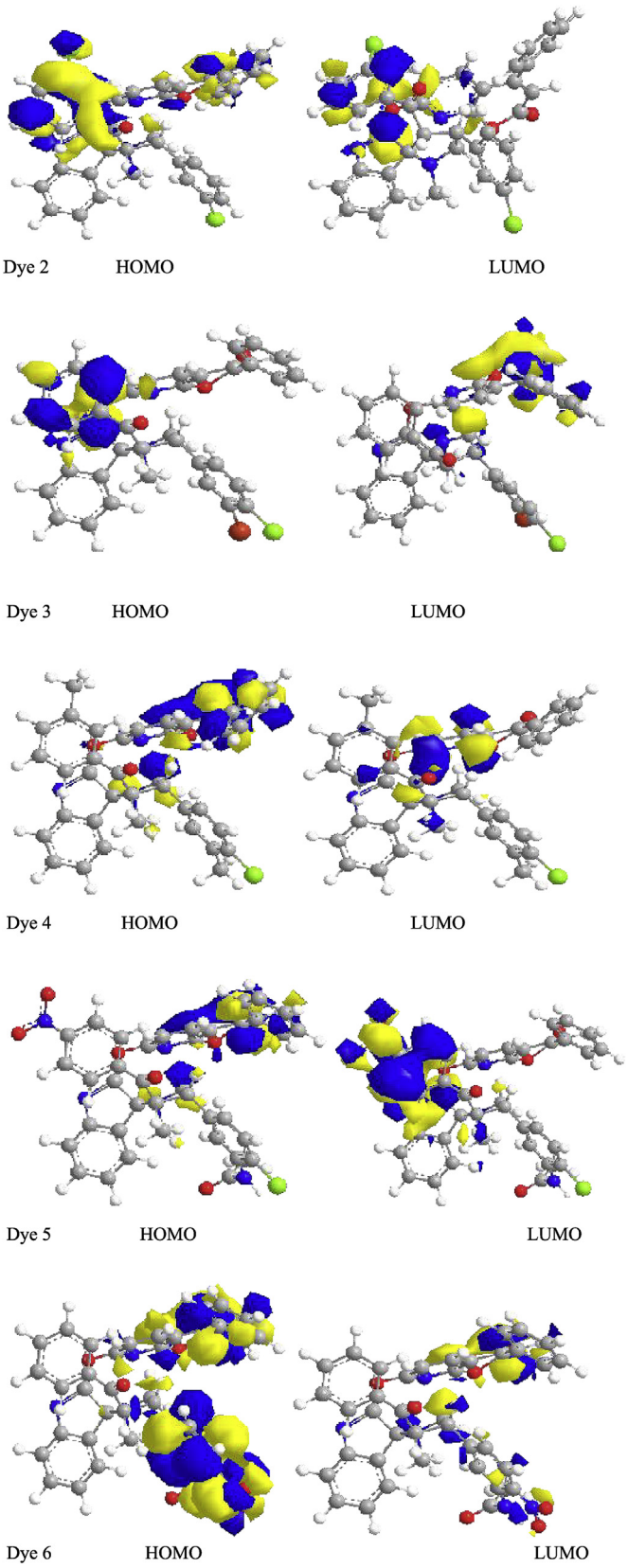

Fig. 1. Outline the molecular orbital of the SACD.

LUMO energy (E_{LUMO}) refers to the electron affinity and its value express the vulnerability of the molecule towards a nucleophilic attack. To obtain these parameters, the molecule must be subjected first to geometry optimization, and then these parameters are calculated. The HOMO and LUMO distributions are displayed in Fig. 4. Evidently, HOMOs are distributed over the Azacoumarin unit, while LUMOs are focused on the indolone moiety, and this is generally for the five compounds. Therefore, Spiro-oxindoline and Azacoumarin moieties are the most active centers in the studied for electron transfer (either electron donation or acceptance of organic compounds towards the interaction with metal surfaces. Compounds having small ΔE values are generally referred to as soft compounds, while those having large values are called hard compounds. In general, soft compounds are more reactive towards metal-additive interactions; being capable of donating electrons easily to metal surface. Generally, for an organic material to interact effectively with metal surface, it must contain heteroatoms rich in non-bonded electrons (free lone pairs) and/or aromatic rings having p-electrons. Heteroatoms and aromatic rings are the major adsorption centers at which electron transfer occurs between the additive and the metal during operating conditions. The synthesized compounds under study are rich in O and N atoms containing free lone pairs of electrons beside double bonds and aromatic rings containing p-electrons. Low-gap-energy compounds generally provide good interaction with perovskite surface because the energy required to remove an electron from the last occupied orbital (HOMO) of the inhibitor will be minimized and it will be easy to donate electrons to the metal. Moreover, such compounds require less energy to be excited and give energy to Pb surface, and they can be easily polarizable more than hard compounds. There are several other various quantum chemical parameters that can help to predict the molecular characteristics of Dye additives such as ionization potential (I), electron affinity (A), absolute electronegativity (χ) and absolute chemical hardness (η) be sure these arrange the binding according Dye **2** < Dye **4** < Dye **3** < Dye **5** < Dye **6**. χ and η are two quantities related to I and A, where $\chi = I+A/2$ and $\eta = I-A/2$, I and A are calculated in turn, from E_{HOMO} and E_{LUMO}, where $I = -E_{HOMO}$ and $A = -E_{LUMO}$. For any two molecules in contact with each other, electrons will be partially transferred from the one of low value to that of higher value. For the studied compounds, χ is generally lower than that of Pb, which is **6** eV, and thus lead- Additive interaction may proceed via electron transfer from the former to the latter. Since soft compounds are preferred for such interactions, one can conclude that Dye **6** is the best candidate for interacting with Pb surface, where it has the highest value of chemical softness (s), which is defined as the inverse of hardness ($s = 1/\eta$) [40]. The electrophilicity ω index is given by the simple expression: $\omega = E^2/\eta$. The electrophilicity ω index encompasses the tendency of an electrophile to acquire an extra amount of electron density, given by binding energy (E) and the resistance of a molecule to exchange electron density with the environment, given by η. Thus, a good electrophile is a species characterized by a high (E) value and a low (η) value. Besides, the maximum number of electrons that an electrophile can acquire is given by the expression: $\Delta N_{max} = E/\eta$. Hence, according to these values, the efficiency order is as follows: Dye**6** > Dye**5** >Dye **4** > Dye**3** > Dye**2**.

4. Conclusions

Five novel Spiro-Azacoumarin derivatives were prepared and studied as additives for improving the oxidation stability of lubricating oils and enhancing the light absorption of perovskite materials. The results obtained in this work, indicate the following:

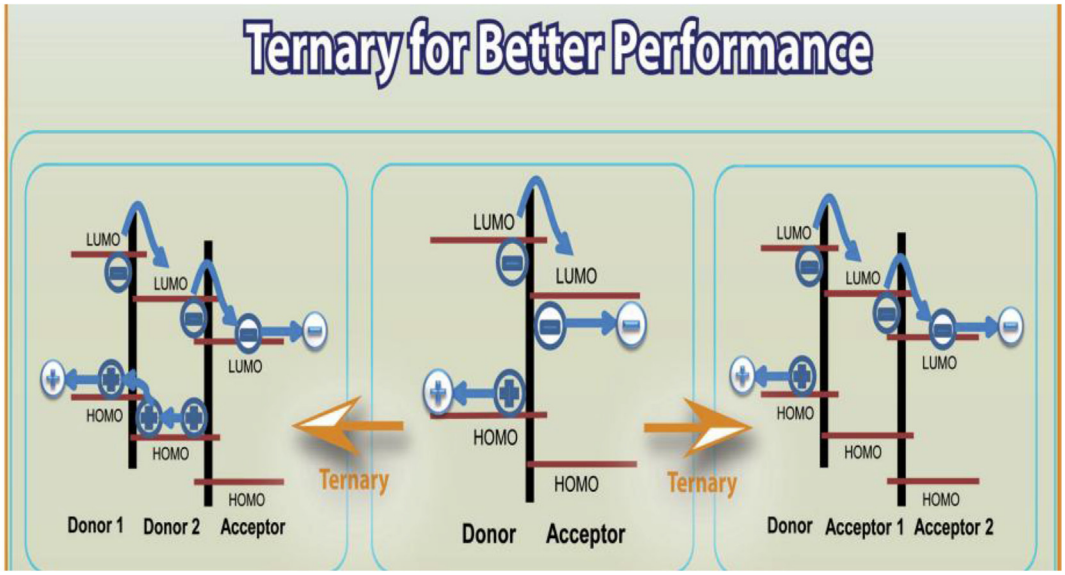

Fig. 2. Outline ternary HOMO-LUMO interaction.

Table 3
TAN variation with oxidation time at different additive concentrations.

Compound	Total acid number, mg KOH/g Sample × 10^2				
	Concentration (ppm)	Oxidation time (h)			
		24	48	72	96
2	200	51.29	67.30	84.10	187.82
	400	63.90	77.32	93.12	191.75
	500	76.40	84.62	105.68	200.32
3	200	36.38	70.81	83.21	177.63
	400	49.12	85.23	100.86	190.72
	500	73.5	96.11	119.96	196.6
4	200	22.97	41.52	68.65	107.85
	400	32.26	53.63	83.99	110.12
	500	44.6	70.45	95.41	164.38
5	200	3.29	19.30	64.10	107.82
	400	9.94	27.32	83.12	131.75
	500	16.40	34.62	95.68	160.32
6	200	2.31	18.81	63.21	113.63
	400	9.10	25.23	79.86	140.72
	500	13.5	36.11	89.96	151.62
Oil (without additive)	–	94	102	120	202

Table 4
Outline the polarizability of Dyes 2–6 through functions of the power 10 (Equation (4)).

Compounds	Polarizability (n) (A^o)	Absorption (α) (ε)	Wavelength (λ) (nm)
Dye 2	4.31778	0.90	520
Dye 3	3.81133	0.90	473
Dye 4	5.88299	0.80	554
Dye 5	7.45313	0.95	494
Dye 6	4.33435	0.85	435

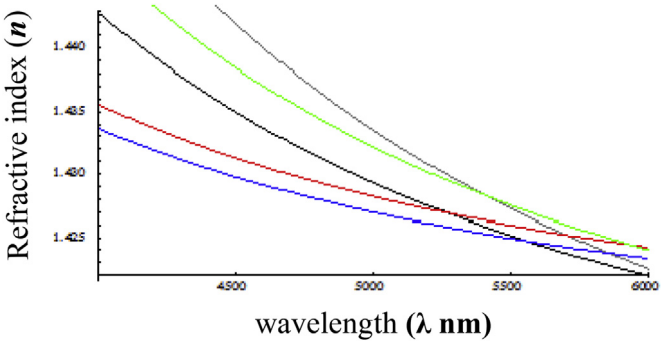

Fig. 3. Outline relation between Refractive index (n) and wavelength λ of Dyes 2-6.

1 The synthesized compounds proved to be successful in controlling the oxidation stability of the base stock oil. The data reveals that the most effective concentration in the case of all compounds (dyes 2–6) is 200 ppm and the efficiency proceed in the order: Dye **6** > Dye **5** > Dye **4** > Dye **3** > Dye **2.**
2 The relation of wavelength, absorption and polarizability are given in three-dimensional. The numerical result gives a good approximation at x to the power 10 and non-linearity depending xy and x^5y. So, these parameters can be confirmed that the sensitized Dyes **4**, **5** and **6** are characterized in range the visible light region and they are having good absorption and polarizability.
3 Then quantum chemical calculations performed for these compounds confirm the obtained experimental results.

As a future perspective, these materials are promising for the energy sector in general context. For lubricating oils, these materials have proven to be efficient as antioxidants that can enhance the oils life-time. In addition, these materials are effective for

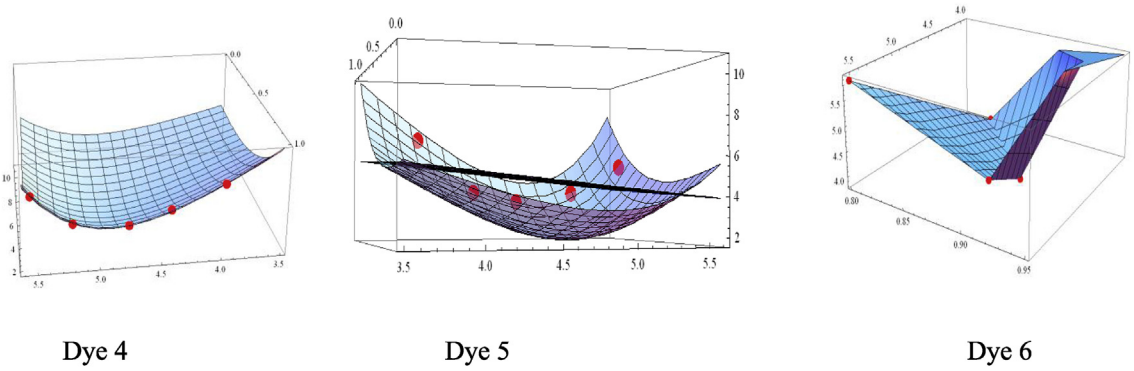

Fig. 4. Outlined the relation among wavelength (X axis), polarizability (Y axis) and absorption (Z-axis).

Table 5
Quantum chemical parameters calculated for the studied compounds.

Compound	E_{HOMO} (eV)	E_{LUMO} (eV)	ΔE (eV)	I (eV)	A (eV)	E_{Bind} (eV)	χ (eV)	η (eV)	S (eV^{-1})	ω	ε	ΔN
(Dye 2)	−4.302	−1.945	2.35	4.302	1.94	−3.123	3.123	2.36	0.424	2.07	0.48	1.32
(Dye 3)	−4.133	−1.945	2.19	4.133	1.95	−3.039	3.039	2.19	0.457	2.11	0.47	1.39
(Dye 4)	−4.428	−1.931	2.50	4.428	1.93	−3.179	3.179	2.50	0.400	2.02	0.49	1.27
(Dye 5)	−4.651	−4.123	0.53	4.651	4.12	−4.387	4.387	0.53	1.894	18.2	0.06	8.31
(Dye 6)	−4.326	−4.071	0.26	4.326	4.07	−4.198	4.198	0.25	3.921	34.6	0.03	16.5

renewable energy technology, i.e. in dye-sensitized solar cell. The quantum chemistry study shows that is a valuable tool in the investigation of the relationship between the structure of lubricants and their properties.

Acknowledgments

The authors would like to extend their sincere appreciation to the faculty of Science, Ain Shams University (ASU) and Egyptian Petroleum Refined Institute (EPRI) for their cooperation in this research.

Appendix A. Supplementary data

Supplementary data to this article can be found online at https://doi.org/10.1016/j.molstruc.2019.02.042.

References

[1] M. Theo, D. Wilfried, Lubricants and Lubrication, second ed., Weinheim VCH Verlag GmbH Co K GaA, 2007, pp. 50–65.
[2] B. Diego, B. Elena, D. Fabio, B. Gemilio, Global risk-based Management of chemical additives production usage and environmental occurrence, Handbook environmental chem (2012) 109–132.
[3] N.S. Ahmed, A.M. Nassar, Lubricating Oil Additives, Tribology-Lubricants and Lubrication, InTech, 2011.
[4] J.S. Basta, A.A. El-Bassoussi, A.A. Salem, M.I. Nessim, M.H. Ahmed, S.K. Attia, Preparation and evaluation of some benzimidazole derivatives as antioxidants for local base oil, Egypt J. Petroleum (2016).
[5] W. Huang, Y. Tan, B. Chen, J. Dong, X. Wang, The binding of antiwear additives to iron surfaces: quantum chemical calculations and tribological tests, Tribol. Int. 36 (2003) 163–168.
[6] V. Jaiswal, R.B. Rastogi, J.L. Maurya, P. Singh, A.K. Tewari, Quantum chemical calculation studies for interactions of antiwear lubricant additives with metal surfaces, RSC Adv. 4 (2014) 13438–13445.
[7] R. Singh, P.K. Singh, B. Bhattacharya, H. Rhee, Review of current progress in inorganic hole-transport materials for perovskite solar cells, Applied Materials Today 14 (2019) 175–200.
[8] Rahul, P.K. Singh, M. Parvaza, S. Ahmed, R.K. Sonker, B. Bhattacharya, Z.H. Khan, Less toxic tin incorporated perovskite solar cell using polymer electrolyte processed in the air, Optik (2018) 166–171.
[9] A. Marrocchi, A. Facchetti, D. Lanari, C. Petrucci, L. Vaccaro, Current methodologies for a sustainable approach to π-conjugated organic semiconductors, Energy Environ. Sci. 9 (2016) 763–786.
[10] A. Robitaille, A. Perea, D. Bélanger, M. Leclerc, Poly(5-alkyl-thieno[3,4-c] pyrrole-4,6-dione): a study of π-conjugated redox polymers as anode materials in lithium-ion batteries, J. Mater. Chem. A 5 (2017) 18088–18094.
[11] C. Morales, D. Borja, J. Maldonado, A. Roa, M. Rodríguez, J. Merinos, A. Castolo, Small molecules derived from Thieno[3,4-c]pyrrole-4,6-dione and their use in solution processed organic solar cells, Molecules 22 (2017) 1607–1619.
[12] F. Lombeck, F. Marx, K. Strassel, S. Kunz, C. Lienert, H. Komber, R. Friend, M. Sommer, C–H selectivity of thiophene-based donor–acceptor–donor monomers in direct arylation polycondensation exemplified by PCDTBT, Polym. Chem. 8 (2017) 4738–4745.
[13] P. Chávez, C. Ngov, P. de Frémont, P. Lévêque, N. Leclerc, Synthesis by direct arylation of thiazole–derivatives: regioisomer configurations–optical properties relationship investigation, J. Org. Chem. 79 (2014) 10179–10188.
[14] S. Erdogan, Z.S. Safi, S. Kaya, D.O. Iş ın, L. Guo, C. Kaya, A computational studyon corrosion inhibition performances of novel quinoline derivatives against the corrosion of iron, J. Mol. Struct. 1134 (2017) 751–761.
[15] G.L.F. Mendonça, S.N. Costa, V.N. Freire, P.N.S. Casciano, A.N. Correia, P.d. Lima-Neto, Understanding the corrosion inhibition of carbon steel and copper insulphuric acid medium by amino acids using electrochemical techniques allied to molecular modelling methods, Corros. Sci. 115 (2017) 41–55.
[16] X. Guo, H. Xin, F. Kim, A. Liyanage, S. Jenekhe, M. Watson, Thieno[3,4-c]pyrrole-4,6-dione-Based Donor–Acceptor conjugated polymers for solar cells, Macromolecules 44 (2011) 269–277.
[17] X. Guo, N. Zhou, S. Lou, J. Hennek, R. Ortiz, M. Butler, P. Boudreault, J. Strzalka, P. Morin, M. Leclerc, et al., Bithiopheneimide dithienosilole dithienogermole copolymers for efficient solar cells: information from structure–property–device performance correlations and comparison to Thieno[3,4-c]pyrrole-4,6-dione Analogues, J. Am. Chem. Soc. 134 (2012) 18427–18439.
[18] J. Pouliot, F. Grenier, J. Blaskovits, S. Beaupré, M. Leclerc, Direct (hetero)arylation polymerization: simplicity for conjugated polymer synthesis, Chem. Rev. 116 (2016) 14225–14274.
[19] A. Hendsbee, J. Sun, W. Law, H. Yan, I. Hill, D. Spasyuk, G. Welch, Synthesis, Self-assembly and solar cell performance of N-annulated perylene diimide non-fullerene acceptors, Chem. Mater. 28 (2016) 7098–7109.
[20] J. Pouliot, L. Mercier, S. Caron, M. Leclerc, Accessing new DPP-based copolymers by direct heteroarylation polymerization, Macromol. Chem. Phys. 214 (2013) 453–457.
[21] A. Payne, S. Li, S. Dayneko, C. Risko, G. Welch, An unsymmetrical non-fullerene acceptor: synthesis via direct heteroarylation, self-assembly, and utility as a low energy absorber in organic photovoltaic cells, Chem. Commun. 53 (2017) 10168–10171.
[22] A. Payne, G. Welch, Optimized synthesis of π-extended squaraine dyes relevant to organic electronics by direct (hetero)arylation and Sonogashira coupling reactions, Org. Biomol. Chem. 15 (2017) 3310–3319.
[23] S. McAfee, J. McCahill, C. Macaulay, A. Hendsbee, G. Welch, Utility of a heterogeneous palladium catalyst for the synthesis of a molecular semiconductor via Stille, Suzuki, and direct heteroarylation cross-coupling reactions, RSC Adv. 5 (2015) 26097–26106.
[24] S. Beaupré, A. Pron, S. Drouin, A. Najari, L. Mercier, A. Robitaille, M. Leclerc, Thieno-, Furo-and Selenopheno[3,4-c]pyrrole-4,6-dione copolymers: effect of

the heteroatom on the electrooptical properties, Macromolecules 45 (2012) 6906–6914.
[25] X. Chen, X. Liu, M. Burgers, Y. Huang, G. Bazan, Green solvent-processed molecular solar cells, Angew. Chem. Int. Ed. 53 (2014) 14378–14381.
[26] L. Rutledge, S. McAfee, G. Welch, Design and computational characterization of non-fullerene acceptors for use in solution-processable solar cells, J. Phys. Chem. A 118 (2014) 7939–7951.
[27] H. Yin, Y. Geng, G. Sun, Z. Su, Theoretical design of perylene diimide dimers with different linkers and bridged positions as promising non-fullerene acceptors for organic photovoltaic cells, J. Phys. Chem. C 121 (2017) 2125–2134.
[28] W. Sha, X. Ren, L. Chen, C. Choy, The efficiency limit of $CH_3NH_3PbI_3$ perovskite solar cells, Appl. Phys. Lett. 106 (2015) 221104–221120.
[29] A. Facchetti, L. Vaccaro, Marrocchi assunta semiconducting polymers prepared by direct arylation polycondensation, Angew. Chem. Int. Ed. 51 (2012) 3520–3523.
[30] M. El-Hashash, S. Rizk, One-pot synthesis of novel spirooxindoles as antibacterial and antioxidant agents, J. Het. Chem. 54 (2017) 1776–1784.
[31] Y. Huang, E. Kramer, A. Heeger, G. Bazan, Bulk heterojunction solar cells: morphology and performance relationships, Chem. Rev. 114 (2014) 7006–7043.
[32] P. Josse, A. Labrunie, C. Dalinot, S. McAfee, S. Dabos-Seignon, J. Roncali, G. Welch, P. Blanchard, C. Cabanetos, Effect of side chains on the electronic and photovoltaic properties of diketopyrrolopyrrole-based molecular acceptors, Org. Electron. 37 (2016) 479–484.
[33] S. Lan, C. Chang, Y. Lu, S. Lin, A. Jen, K. Wei, Side chain structure affects the molecular packing and photovoltaic performance of oligothiophene-based solution-processable small molecules, RSC Adv. 5 (2015) 67718–67726.
[34] B. Kan, Q. Zhang, F. Liu, X. Wan, Y. Wang, W. Ni, X. Yang, M. Zhang, T. Russell, et al., Small Molecules Based on Alkyl/Alkylthio-thieno[3,2-b]thiophene-substituted benzo[1,2-b:4,5-b]dithiophene for solution-processed solar cells with high performance, Chem. Mater. 27 (2015) 8414–8423.
[35] K. Graham, C. Cabanetos, J. Jahnke, M. Idso, A. El Labban, G. Ngongang, et al., Importance of the donor fullerene intermolecular arrangement for high efficiency organic photovoltaics, J. Am. Chem. Soc. 136 (2014) 9608–9618.
[36] H. Hu, K. Jiang, G. Yang, J. Liu, Z. Lin, H. Liu, Y. Zhao, Terthiophene-based D–A polymer with an asymmetric arrangement of alkyl chains that enables efficient polymer solar cells, J. Am. Chem. Soc. 137 (2015) 14149–14157.
[37] Y. Kim, S. Choulis, J. Nelson, D. Bradley, J. Durrant, Device annealing effect in organic solar cells with blends of regioregular poly(3-hexylthiophene) and soluble fullerene, Appl. Phys. Lett. 86 (2005), 063502.
[38] R. Aïch, Solvent effect and device optimization of diketopyrrolopyrrole and carbazole copolymer based solar cells, Org. Electron. 11 (2010) 1053–1058.
[39] J. Seo, Y. Sun, C. Takacs, J. Seifter, A. Heeger, Inverted polymer solar cells integrated with a low temperature annealed sol-gel-derived ZnO film as an electron transport layer, Adv. Mater. 23 (2011) 1679–1683.
[40] N. An, B. Zhuang, M. Li, Y. Lu, Z. Wang, Combined theoretical and experimental study of refractive indices of water acetonitrile salt systems, J. Phys. Chem. 119 (2015) 10701–10709.
[41] F. El-Taib Heakal, S.K. Attia, S.A. Rizk, M.A. Abou Essa, A.E. Elkholy, Synthesis, characterization and computational chemical study of novel pyrazole derivativesas anticorrosion and antiscalant agents, J. Mol. Struct. 1147 (2017) 714–724.
[42] S. Rizk, A. El-Naggar, A. El-Badawy Synthesis, Spectroscopic characterization and computational chemical study of 5-cyano-2-thiouracil derivatives as potential antimicrobial agents, J. Mol. Struct. 1155 (2018) 720–733.
[43] S. Rizk, G. Elsayed, M. El-Hashash, One-pot synthesis, spectroscopic characterization and DFT study of novel 8-azacoumarin derivatives as eco-friendly insecticidal agents, J. Iran. Chem. Soc. 15 (2018) 2093–2105.